

This document contains a post-print version of the paper

Influence of Air Cooling Jets on the Steady-State Shape of Strips in Hot Dip Galvanizing Lines

authored by M. Saxinger, A. Steinböck, M. Baumgart, P. Kerschbaummayr, and A. Kugi
and published in *Proceedings of the 4th IFAC Workshop on Mining, Mineral and Metal Processing (MMM)*.

The content of this post-print version is identical to the published paper but without the publisher's final layout or copy editing. Please, scroll down for the article.

Cite this article as:

M. Saxinger, A. Steinböck, M. Baumgart, P. Kerschbaummayr, and A. Kugi, "Influence of air cooling jets on the steady-state shape of strips in hot dip galvanizing lines", in *Proceedings of the 4th IFAC Workshop on Mining, Mineral and Metal Processing (MMM)*, vol. 48, Oulu, Finland, 25.08.-28.08. 2015, pp. 143–148. DOI: [10.1016/j.ifacol.2015.10.093](https://doi.org/10.1016/j.ifacol.2015.10.093)

BibTex entry:

```
% This file was created with JabRef 2.8.1.  
% Encoding: Cp1252
```

```
@inproceedings{acinpaper,  
  author = {Saxinger, M. and Steinböck, A. and Baumgart, M. and Kerschbaummayr, P. and Kugi, A.},  
  title = {Influence of Air Cooling Jets on the Steady-State Shape of Strips in Hot Dip Galvanizing Lines},  
  booktitle = {Proceedings of the 4th IFAC Workshop on Mining, Mineral and Metal Processing (MMM)},  
  month = {25.08.-28.08.},  
  year = {2015},  
  volume = {48},  
  address = {Oulu, Finland},  
  number = {17},  
  pages = {143--148},  
  doi = {10.1016/j.ifacol.2015.10.093},  
  issn = {2405-8963}  
}
```

Link to original paper:

<http://dx.doi.org/10.1016/j.ifacol.2015.10.093>

Read more ACIN papers or get this document:

<http://www.acin.tuwien.ac.at/literature>

Contact:

Automation and Control Institute (ACIN)
Vienna University of Technology
Gusshausstrasse 27-29/E376
1040 Vienna, Austria

Internet: www.acin.tuwien.ac.at
E-mail: office@acin.tuwien.ac.at
Phone: +43 1 58801 37601
Fax: +43 1 58801 37699

Copyright notice:

This is the authors' version of a work that was accepted for publication in *Proceedings of the 4th IFAC Workshop on Mining, Mineral and Metal Processing (MMM)*. Changes resulting from the publishing process, such as peer review, editing, corrections, structural formatting, and other quality control mechanisms may not be reflected in this document. Changes may have been made to this work since it was submitted for publication. A definitive version was subsequently published in M. Saxinger, A. Steinböck, M. Baumgart, P. Kerschbaummayr, and A. Kugi, "Influence of air cooling jets on the steady-state shape of strips in hot dip galvanizing lines", in *Proceedings of the 4th IFAC Workshop on Mining, Mineral and Metal Processing (MMM)*, vol. 48, Oulu, Finland, 25.08.-28.08. 2015, pp. 143–148. doi: [10.1016/j.ifacol.2015.10.093](https://doi.org/10.1016/j.ifacol.2015.10.093)

Influence of Air Cooling Jets on the Steady-State Shape of Strips in Hot Dip Galvanizing Lines *

M. Saxinger* A. Steinboeck** M. Baumgart*
P. Kerschbaummayr*** A. Kugi*

* Christian Doppler Laboratory for Model-Based Process Control in the Steel Industry, Automation and Control Institute, Vienna University of Technology, Austria, (e-mail: {saxinger, baumgart, kugi}@acin.tuwien.ac.at).

** Automation and Control Institute, Vienna University of Technology, Austria (e-mail: steinboeck@acin.tuwien.ac.at)

*** voestalpine Stahl GmbH, Linz, Austria, (e-mail: peter.kerschbaummayr@voestalpine.com)

Abstract: The influence of air cooling jets on the steady-state shape of the strip in hot dip galvanizing lines is investigated. For this purpose, the force characteristic of a single nozzle is measured by a laboratory flow simulator. This approach differs from conventional methods, where typically, CFD simulations are used. Based on the air cooler force characteristic the stability of the equilibrium points is investigated and the influence of different types of boundary conditions, tensile loads, strip thicknesses, and cooler fan speeds is examined.

Keywords: Mechanical system, Static models, Moving objects, Distributed-parameter system, Mathematical model, Stability analysis, Steel industry, Numerical simulation, Equilibrium.

1. INTRODUCTION

In hot dip galvanizing lines, like the one shown in Fig. 1, cold-rolled steel strip is coated in a bath of molten zinc. The strip is heated in an annealing furnace and guided by the sink roll. It leaves the zinc bath after passing the correction and stabilization roll. Above the zinc pool, gas wiping dies are mounted across the width of the strip to reduce the thickness of the zinc layer to a certain value. Cooling arrays consisting of four cooling sections are located at the upper part of the galvanizing line. They guarantee a solidified zinc layer once the strip reaches the tower roll.

Experience over many years has shown that cooling jets can influence the stability of the strip motion, in particular when thinner and broader strips are processed. Moreover, in special cases even unwanted vibrations of the strip may be induced or the strip may collide with the nozzles of the cooling section. Many studies on the modeling of axially moving beams and membranes are available (Shin et al., 2006; Steinboeck et al., 2015; Pellicano and Vestroni, 2000; Antman, 2006; Chen, 2005; Marynowski and Kapitaniak, 2014), but up to the authors' knowledge no systematic investigations of the influence of the cooling array air jets on the stability of the strip in hot dip galvanizing lines can

* The financial support by the Austrian Federal Ministry of Science, Research and Economy and the National Foundation for Research, Technology and Development is gratefully acknowledged. The second author gratefully acknowledges financial support provided by the Austrian Academy of Sciences in the form of an APART-fellowship at the Automation and Control Institute of Vienna University of Technology.

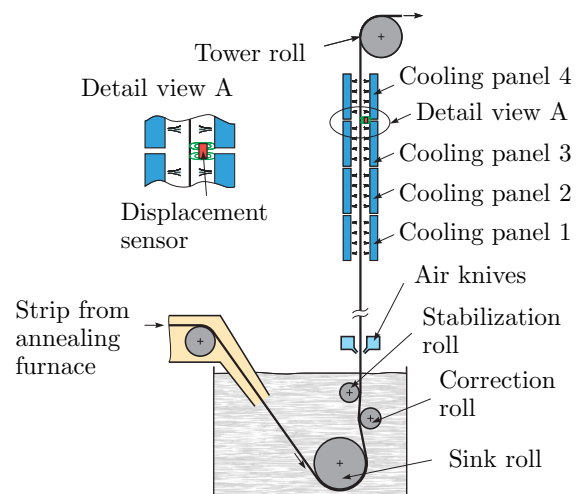


Fig. 1. A typical hot dip galvanizing line with a cooler array consisting of four panels.

be found in the literature. The effect of the air cooling jets on the shape and on the stability of the strip is investigated in this paper.

For this, three eddy current sensors were used to examine the interaction between the cooler fan speed and the relative displacement of the strip. Two displacement sensors were assembled between the cooling sections 3 and 4 in order to measure the displacement at the outer edges of the strip: One at the drive side (DS), the other one at the operator side (OS). The third sensor was located in the middle of the strip (MI). The fan speed n_2 of cooler 2 was

varied, all other fan speeds n_1 , n_3 and n_4 and the most important parameters of the plant were held constant for this experiment. Fig. 2 shows the measured relationship between the fan speed n_2 and the displacement Δd of the strip for both increasing and decreasing fan speeds. The displacement Δd of each sensor is measured relative to its starting position. Displacements Δd for increasing fan speeds (up) are shown with bold lines and decreasing fan speeds are designated with thin lines. The fan speed was kept constant at a certain level for a few seconds and for this time interval the displacement measurements were averaged. The averaged data points are highlighted with markers. These measurement results clearly show that the strip displacement is influenced by the fan speed setting, although the absolute position of the strip is unknown. Ad-

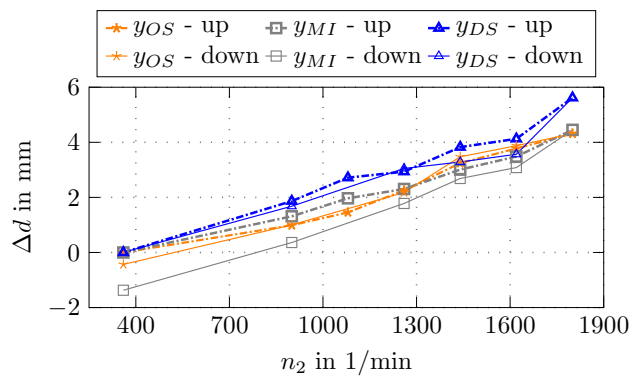


Fig. 2. Relative displacement Δd of the strip for different sensor positions.

ditional measurements showed a clear correlation between the relative pressure p in the supply duct of the cooling jets (hereinafter denoted as pressure p) and the fan speed n of the respective blower. The pressure drop inside a cooling section can be considered as negligible. This simplification is supported by a cooler test run with twelve pressure sensors mounted at different positions in the cooling section. By means of a least-squares approximation the unknown parameters of the semi-empirical relation

$$p = c_1 n + c_2 n^2 \quad (1)$$

are determined as $c_1 = 1.6785 \cdot 10^{-4}$ mbar min and $c_2 = 1.1847 \cdot 10^{-5}$ mbar min². In order to study the pressure force of an impinging nozzle jet on the strip a flow simulator was developed.

2. FLOW SIMULATOR

A cooling section with the parameters in Table 1 is outlined in Fig. 3. All pipes are supplied by an air blower from the DS. With negligible pressure drop inside the pipes of one section, the air stream through all nozzles must be the same. Furthermore, the flow conditions after the fluid leaves the nozzle are similar. This assumption is supported by the geometry of the cooling section, where the fluid can only escape to the rear side. For a proper analysis of the force characteristic, a laboratory flow simulator with three nozzles was setup. The mechanism of an impinging jet force on a plate was analyzed for various distances h_s between the nozzle and the plate/strip and various relative pipe pressures p . Several design aspects have been taken

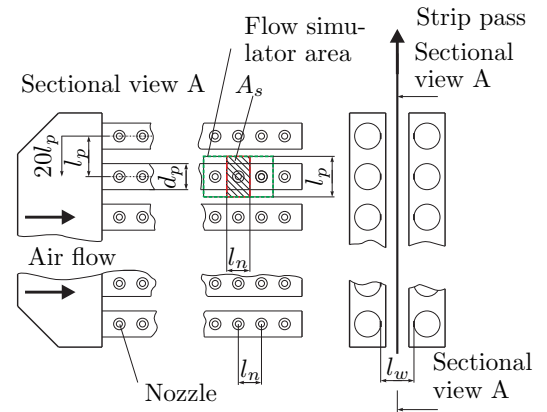


Fig. 3. Sketch of one cooling panel. The flow simulator area is marked with dashed lines. All nozzles have the same diameter d_n .

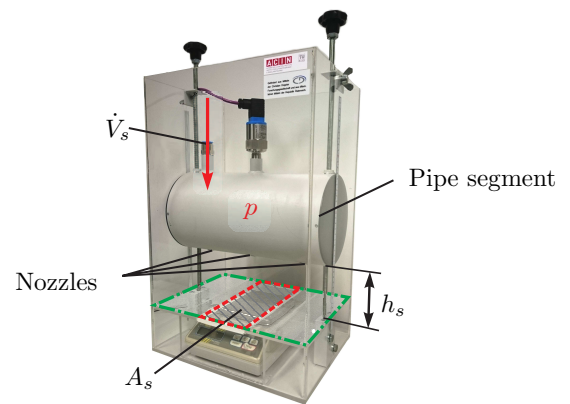


Fig. 4. Picture of flow simulator.

into account. First of all, the force application surface is in line with the associated area of the strip at the real cooling panel. Also, the diameter of the pipe is equal to the real cooling pipe and the lateral distance between neighboring nozzles is the same as in the real system. The vertical distance l_p between the single pipes equals the depth of the simulator. Thus the channel for the back-flow is also identical to the real cooling section. In order to account for the stream interactions between neighboring nozzles, at least three nozzles were used. Friction alongside the simulator wall can be neglected as a result of low fluid velocity at the wall. The flow simulator is shown in Fig. 4.

Fig. 5 shows the measured force F_s acting on the area A_s as a function of the pressure p depending on the distance h_s . An interesting feature can be seen in Fig. 6: In normal operating situations ($h_s > 1$ cm), there is no influence of the distance h_s on the flow rate \dot{V}_s of air. During the measurements, h_s was varied from 0 to l_w .

Table 1. Parameters of cooling section.

Parameter	Value	Unit
d_p	168.3	mm
l_p	250	mm
l_n	110	mm
l_w	250	mm
d_n	17.5	mm

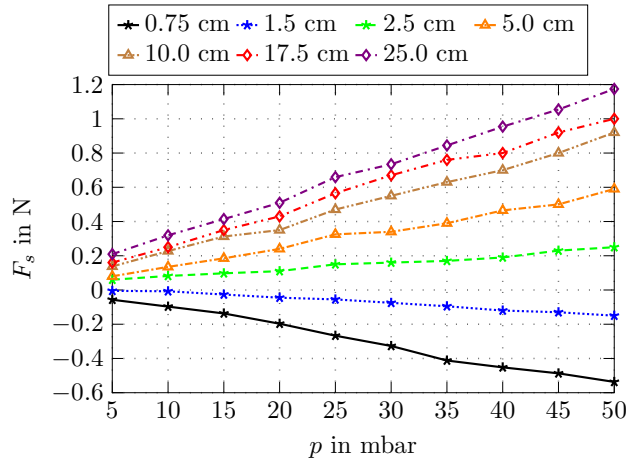


Fig. 5. Force of impinging jet F_s depending on distance h_s .

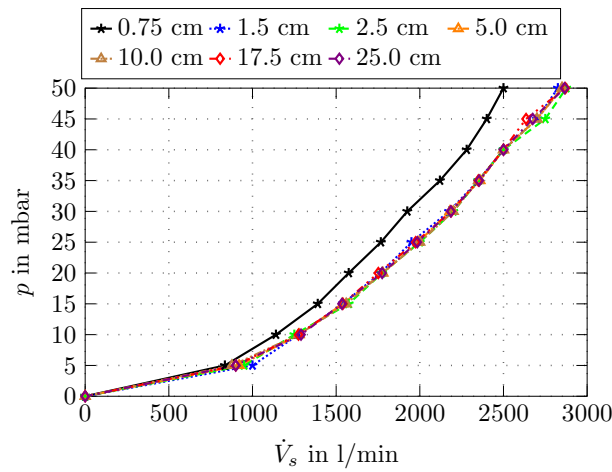


Fig. 6. An influence of the distance h_s on the flow rate \dot{V}_s occurs only at small distances < 1 cm.

3. MODEL OF AXIALLY MOVING STRIP WITH COOLING PANELS

3.1 Cooling Sections

To transfer the results of the simulator to the nozzles of the plant, an offset displacement $w = h_s - l_w/2$ must be introduced, see Figs. 4 and 3 for details. Based on the results obtained so far, in particular Fig. 5, a semi-empirical relation of the form

$$F_s(p, w) = (p + c_3 p^2) (c_4 e^{-c_5 w} + c_6 w + c_7) \quad (2)$$

can be extracted, with the parameters c_3 , c_4 , c_5 , c_6 , and c_7 according to Table 2, see Fig. 7. For a nozzle pair consisting of two vis-à-vis nozzles, the resulting pressure load on the area A_s is then derived as

$$q_c(p, w) = \frac{F_s(p, w + w_0) - F_s(p, -w - w_0)}{A_s}. \quad (3)$$

Here, w_0 is a constant transversal offset displacement of the strip. See Fig 8 for more details. It is assumed that all nozzle pairs over the whole width of the strip exert the same force on the strip.

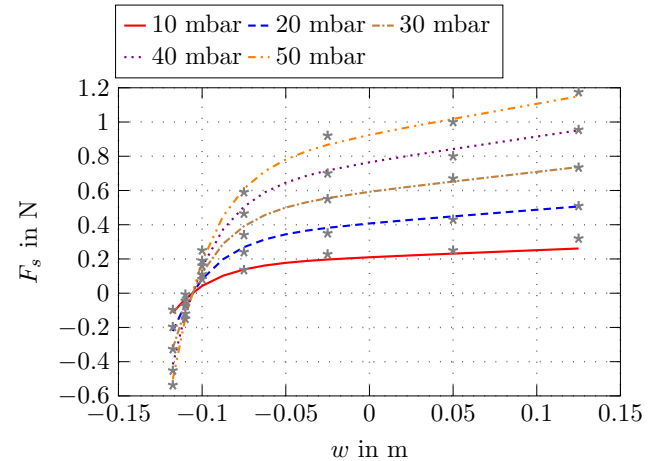


Fig. 7. Force of impinging nozzle jet F_s depending on pressure p in the pipe. Measurement data is highlighted by markers.

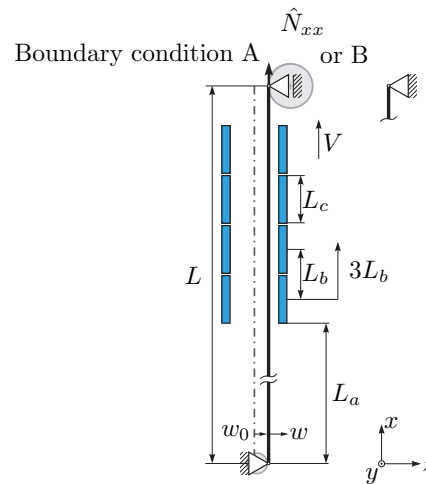


Fig. 8. Schematic of strip and cooler dimensions of the plant.

3.2 Steady-State Model of an Axially Moving Strip

In the following, partial derivatives are denoted by $(\cdot)' = \partial(\cdot)/\partial x$ and $(\dot{\cdot}) = \partial(\cdot)/\partial t$. Furthermore, $u = u(x)$ and $w = w(x)$ are the displacements in longitudinal and transversal direction, respectively. A schematic of the strip influenced by the cooling array with all boundary conditions is given in Fig. 8. The Euler-Lagrange equation for the steady-state displacement u in x -direction (also denoted as in-plane displacement) obtained from (Shin et al., 2006; Reddy, 2006) reads as

$$\rho A V^2 u'' - N'_{xx} = 0, \quad (4)$$

Table 2. Parameters of impinging jet force characteristic.

Parameter	Value	Unit
c_3	$-2.8969 \cdot 10^{-5}$	1/Pa
c_4	$-1.6449 \cdot 10^{-6}$	m^2
c_5	43.9435	1/m
c_6	$4.0861 \cdot 10^{-4}$	m
c_7	$2.1788 \cdot 10^{-4}$	m^2

with the boundary conditions at the bottom edge

$$u(0) = 0 \quad (5)$$

and at the upper edge

$$N_{xx}(L) = \hat{N}_{xx} \quad (6)$$

for a strip with prescribed tensile load (boundary condition A) or

$$u(L) = \hat{u}_L = \frac{L\hat{N}_{xx}}{EA} \quad (7)$$

for a geometrical boundary condition, where the strip is preloaded with the force \hat{N}_{xx} and then fixed (boundary condition B), see Fig. 8. In (4), N_{xx} is referred to as the tensile force (also denoted as membrane force). The strip velocity V is assumed to be constant, and w_0 is a displacement offset of the strip in z -direction. The Euler-Lagrange equation for the steady-state displacement w in z -direction (out-of-plane displacement) takes the form (Shin et al., 2006; Reddy, 2006)

$$\rho AV^2 w'' - M''_{xx} - (N_{xx} w')' - q = 0, \quad (8)$$

with equal boundary conditions at the bottom and the upper edge. They can be written as

$$w(0) = w(L) = w_0 \quad \text{and} \quad M_{xx}(0) = M_{xx}(L) = 0. \quad (9)$$

Rotation with respect to the y -axis is free. In (8), M_{xx} represents the bending moment. With q as a transversal load acting on the strip, the pressure load q_c induced by the cooler sections can be considered according to (3). Furthermore, ρ is the mass density and A the cross sectional area of the strip. Thus ρA denotes the mass density per unit length of the strip. The expression $\rho AV^2 w''$ represents the centrifugal force.

With the geometrically nonlinear strain relation ϵ and the curvature κ of the strip,

$$\epsilon(x) = u' + \frac{1}{2}(w')^2 \quad \text{and} \quad \kappa(x) = w'', \quad (10)$$

the stress resultants for free transversal contraction can be written as

$$N_{xx}(x) = EA\epsilon \quad \text{and} \quad M_{xx}(x) = -\frac{Ebh^3}{12}\kappa, \quad (11)$$

with Young's modulus E , the strip width b and the strip thickness h . Due to (10), transversal and longitudinal displacements are coupled.

3.3 Stability of Equilibrium Points

For the proof of asymptotic stability, a dynamic model of the strip is required. In order to do so, (8) was extended to a dynamic model as given in (Shin et al., 2006; Reddy, 2006; Steinboeck et al., 2015)

$$\rho A (\ddot{w} + 2V\dot{w}' + V^2 w'') - M''_{xx} - (N_{xx} w')' - q + c_w \dot{w} = 0, \quad (12)$$

with the additional expressions $\rho A \ddot{w}$ as the acceleration force, $\rho A 2V\dot{w}'$ as the Coriolis force and $c_w \dot{w}$ is a linear damping force. Due to the assumption of small amplitudes, high frequencies and fast decaying in-plane vibrations, the in-plane dynamics was neglected. This assumption leads to a quasi-static relationship at every time step between the boundary condition (6) or (7), the w - and the u -displacement field.

4. NUMERICAL RESULTS

The problem that has to be solved consists of the partial differential equations (4) and (8) and the related boundary conditions (5), (6) or (7) and (9). For a numerical solution of the problem (4) and (8), a spatial discretization of the model is necessary. In longitudinal direction, the strip is divided into finite elements of equal length. For each element, the Galerkin weighted residual method is used for both in-plane and out-of-plane motion. As trial functions, Hermite polynomials are employed. They can be easily adapted to the different boundary conditions A and B of the strip. Before solving the algebraic equations gained from the Galerkin method, it is useful to normalize all Galerkin coefficients. The normalized nonlinear system is then solved with the Newton-Raphson method in combination with a line search method as described by Shearer and Cesnik (2006).

For all simulations, the parameter values were chosen as follows: The length of the strip $L = 56.5$ m is discretized with 60 elements, the width is $b = 1.65$ m, and a constant strip velocity $V = 105$ m/min is assumed. The material parameters of the strip are the mass density $\rho = 7850$ kg/m³ and Young's modulus $E = 1.8 \cdot 10^{11}$ N/m². The geometry of the cooling array is defined by $L_a = 34.1025$ m, $L_b = 5.205$ m and $L_c = 5$ m. The damping factor c_w (only used for the investigations of the stability of the equilibrium) is assumed to be 16.5 N s/m². Parameters like strip thickness h , tensile resp. prestress load \hat{N}_{xx} , pressure p of the cooler pipe and the offset w_0 may vary from simulation to simulation.

For simplification, all cooling sections are held on equal pressure level for every simulation. Simulations without an offset yield solutions that are symmetrical with respect to the x -axis. Therefore, only the solution for one side (one sign of w) is visualized in the following. Furthermore, a more general representation is obtained using the specific load \hat{N}_{xx}/b .

4.1 Types of Equilibria

For the proof of asymptotic stability, an early lumping approach was used. After the spatial discretization with the Galerkin method, the ordinary differential equation and the algebraic equation gained from (12) and (4) can be written as

$$\dot{\mathbf{w}} = \mathbf{f}(\bar{\mathbf{w}}, \mathbf{u}) \quad \text{and} \quad \mathbf{0} = \mathbf{g}(\mathbf{w}, \mathbf{u}), \quad (13)$$

with the vector-valued functions \mathbf{f} and \mathbf{g} and the state vector $\bar{\mathbf{w}} = [\mathbf{w}, \dot{\mathbf{w}}]^T$. The vectors \mathbf{w} and \mathbf{u} contain the Galerkin coefficients whereas \mathbf{f} and \mathbf{g} result from the boundary conditions (5), (6) or (7) and (9). A linearization of the nonlinear system (13) at the equilibrium is performed and the normalized eigenvalues of the linear system are computed. The eigenvalue with the largest real part is denoted by e_s . If e_s has a positive real part, the system (12) and (4) with the related boundary conditions is unstable.

Three different types of equilibria are observed depending on the existence of one or two equilibria for non-negative displacement w in the range $0 \leq w \leq l_w/2$. For simplicity, a vanishing offset $w_0 = 0$ is assumed.

- One unstable equilibrium $w = 0$ (case 1): The entire area of the permitted cooler range is unstable. This case can occur for moderate tensile loads (boundary condition A) or prestresses (boundary condition B) \hat{N}_{xx} . A slight deviation from $w = 0$ causes w to grow until the strip collides.
- One stable equilibrium $w = 0$ (case 2): The entire area of the permitted cooler range belongs to the region of attraction of the equilibrium. A high value \hat{N}_{xx} leads to this kind of equilibrium.
- Two equilibria $w = 0$ and $w \neq 0$ (case 3): The inner equilibrium $w = 0$ is always stable and the outer one $w \neq 0$ is always unstable. The region of attraction of the stable (inner) equilibrium contains the range from $w = 0$ to the outer unstable equilibrium.

Example 1: For the last case, the influence of the strip thickness h and the tensile load \hat{N}_{xx} on the unstable equilibrium shape is shown in Fig. 9. The offset shift of the strip is set to $w_0 = 0$ and the cooler pipe overpressure is $p = 40$ mbar. Based on (1), the associated cooler fan speed is approximately $n = 1830$ 1/min.

For $\hat{N}_{xx}/b = 30$ kN/m, two equilibria are observed (case 3): The inner one $w = 0$ is stable ($e_s = -0.47$) and the outer one $w \neq 0$ is unstable ($e_s = 5.36$). The same applies to 40 kN/m: The equilibrium $w = 0$ is stable ($e_s = -0.41$) and the other one $w \neq 0$ is unstable ($e_s = 6.76$). Both unstable equilibria are shown in Fig. 9. For 30 kN/m an estimation of the region of attraction is shown as a shaded area. The cooler array is shown as gray shaded box.

For 55 kN/m, only one stable equilibrium $w = 0$ (case 2) with $e_s = -0.35$ exists. The strip cannot become unstable for the values w permitted by the cooler array.

The low tensile load of 15 kN/m leads to one unstable equilibrium $w = 0$ (case 1) with $e_s = 1.57$. This operating condition must be avoided.

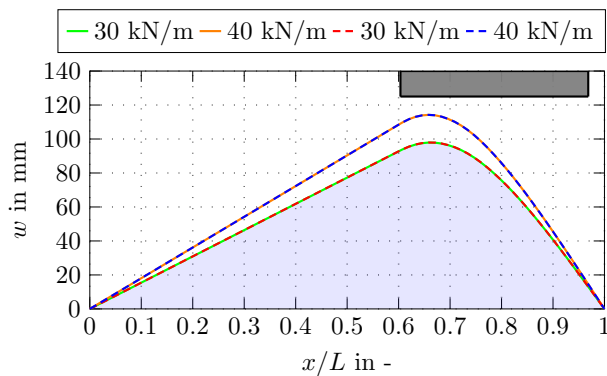


Fig. 9. Unstable equilibria for boundary condition A and various values \hat{N}_{xx}/b (solid line: $h = 1.5$ mm, dashed line: $h = 1$ mm).

4.2 Influence of the Boundary Condition

Henceforth the equilibrium $w = 0$ is not considered. It is analyzed how the shape of the unstable equilibrium

(case 3) changes depending on the thickness h , the boundary condition A or B, and the load \hat{N}_{xx} . Furthermore, the case of using the same prestress displacement \hat{u}_L for all strips with different thicknesses is examined.

Example 2: For boundary condition A with a constant tensile load, the strip thickness h has no noticeable influence on the equilibrium. In contrast, however, the tensile load \hat{N}_{xx} has a significant effect on the equilibrium as can be seen in Fig. 9.

The situation is different for boundary condition B. After prestressing the strip with a total force \hat{N}_{xx} , a certain displacement \hat{u}_L appears depending on the strip thickness. This unique displacement value is fixed at the upper edge, i.e., $u(L) = \hat{u}_L$. For an additional strip extension due to a transversal displacement w , a thicker strip will exercise a higher resetting force. Therefore, an equilibrium will occur slightly further away from the x -axis compared to a thinner strip because the destabilizing effect of the cooler array must also be greater. See the examples shown in Fig. 10 for more details.

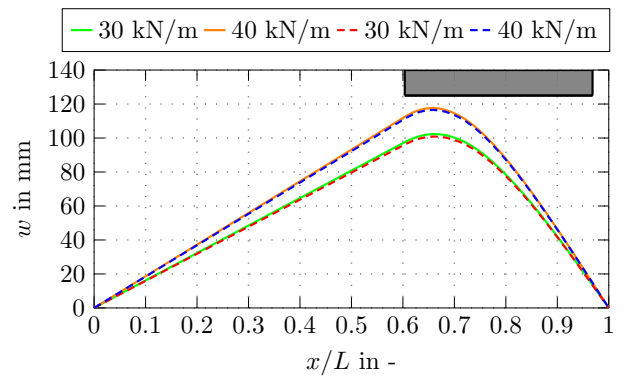


Fig. 10. Unstable equilibria for boundary condition B and various values of \hat{N}_{xx}/b (solid line: $h = 1.5$ mm, dashed line: $h = 1$ mm).

Finally, the same reference displacement $\hat{u}_L = 6.7$ mm is chosen for different strips. According to (7), this displacement would occur for a 1 mm thick and 1.65 m wide strip with a tensile load of 35 kN. The thinnest strip would collide with the cooler array in case of a small disturbance (stability case 1). The remaining two strips will stay stable inside the region of attraction of the stable equilibrium $w = 0$ (case 3). See the remarkable difference between Figs. 10 and 11 which is only caused by the difference of the boundary condition \hat{u}_L .

4.3 Influence of Pressure and Cooler Fan Speed

Example 3: The influence of the cooler pressure on the equilibrium $w \neq 0$ is investigated using the pressure levels [10, 25, 40] mbar. They correspond to the cooler fan speeds [912, 1446, 1830] 1/min, see (1). The simulation results for a thin strip with thickness $h = 0.5$ mm and a tensile load of 20 kN/m (boundary condition A) are shown in Fig. 12. For $p = 10$ mbar, only the equilibrium $w = 0$ exists within the permitted range of the cooler array. The system (13) is linearized about this equilibrium. With $e_s = -1.01$, case

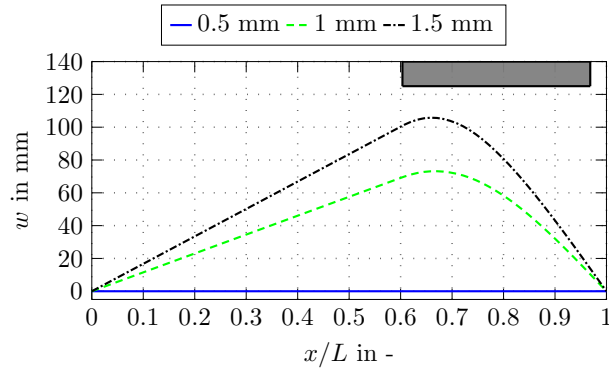


Fig. 11. Unstable equilibria for different strips preloaded by the same displacement \hat{u}_L .

2 occurs and the complete range belongs to the region of attraction of this equilibrium.

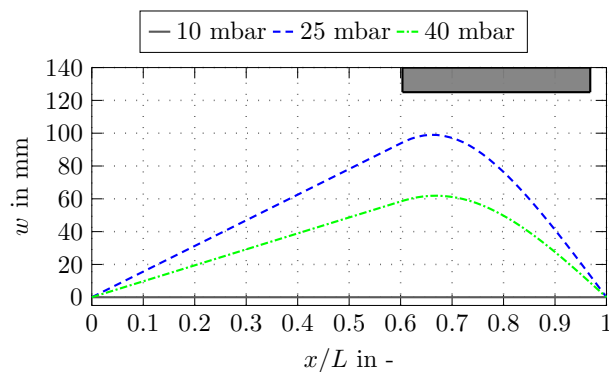


Fig. 12. Stable equilibria for boundary condition A (constant tensile load) and different cooler loads.

4.4 Influence of an Offset Shift

Example 4: An offset shift w_0 may be caused by a misalignment between the ideal strip pass line and the cooling sections. The influence on the stable equilibrium position (case 3) for a strip with thickness $h = 1$ mm and a constant tensile load (boundary condition A) of 35 kN/m is shown in Fig. 13. The cooler pressure is set to 25 mbar.

Even a minor offset shift is causing a big shift of the stable equilibrium in transversal direction. A positive offset will lead to a drift in positive direction and vice versa. This is a direct consequence of the destabilising effect of the cooler array. The outer equilibria are also affected due to the offset shift. For $w \geq 0$, a positive offset w_0 will move the unstable equilibrium further inwards or, equivalently, it will shrink the region of attraction. The unstable equilibrium for $w \leq 0$ will be pushed outwards. Depending on the tensile load \hat{N}_{xx} and on the pressure level p , the entire negative side becomes the region of attraction of the stable equilibrium $w = 0$ in many cases. The unstable equilibria are not shown in this paper.

5. CONCLUSIONS

The most important findings of this study are summarized in the following:

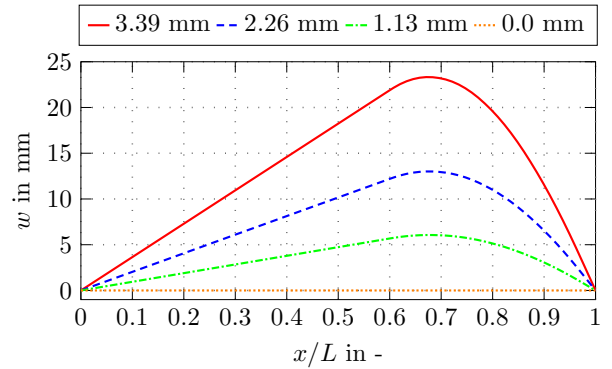


Fig. 13. Stable equilibria for boundary condition A and various offset shifts w_0 .

- Depending on different plant parameters, e.g., the tensile load \hat{N}_{xx} and the pressure level p , three different types of equilibria are observed.
- It is necessary that the inner equilibrium is a stable one to ensure a proper strip processing. Otherwise, the strip will collide with the cooler array. The best way to keep the equilibrium stable is to increase the tensile load \hat{N}_{xx} .
- For a constant tensile load (boundary condition A), the strip thickness h has virtually no effect on the equilibrium. This does not apply to the preloaded and fixed strip (boundary condition B).
- Small imperfections, which lead to an offset shift w_0 of the strip, can have a huge impact on the stability.

REFERENCES

- Antman, S. (2006). *Nonlinear Problems of Elasticity*. Applied Mathematical Sciences. Springer.
- Chen, L.Q. (2005). Analysis and control of transverse vibrations of axially moving strings. *Applied Mechanics Reviews*, 58(2), 91–116.
- Marynowski, K. and Kapitaniak, T. (2014). Dynamics of axially moving continua. *International Journal of Mechanical Sciences*, 81, 26–41.
- Pellicano, F. and Vestroni, F. (2000). Non-linear dynamics and bifurcations of an axially moving beam. *Journal of Vibration and Acoustics*, 122, 21–30.
- Reddy, J. (2006). *Theory and Analysis of Elastic Plates and Shells, Second Edition*. Series in Systems and Control. Taylor & Francis.
- Shearer, C. and Cesnik, C. (2006). Modified generalized α method for integrating governing equations of very flexible aircraft. In *Proceedings of the 47th AIAA/ASME/ASCE/AHS/ASC Structures, Structural Dynamics, and Materials Conference*. Newport, Rhode Island, USA.
- Shin, C., Chung, J., and Yoo, H.H. (2006). Dynamic responses of the in-plane and out-of-plane vibrations for an axially moving membrane. *Journal of Sound and Vibration*, 297(35), 794–809.
- Steinboeck, A., Baumgart, M., Stadler, G., Saxinger, M., and Kugi, A. (2015). Dynamical models of axially moving rods with tensile and bending stiffness. In *8th Vienna International Conference on Mathematical Modelling (IFAC)*. Vienna, Austria.